Lab on a Chip

TUTORIAL REVIEW

View Article Online
View Journal | View Issue

Cite this: *Lab Chip*, 2016, **16**, 4047

Micro-/nanoscale electroporation

Lingqian Chang,†[a] Lei Li,†[b] Junfeng Shi,†[c] Yan Sheng,[d] Wu Lu,[e] Daniel Gallego-Perez*[af] and Ly James Lee*[acd]

Received 4th July 2016,
Accepted 19th September 2016

DOI: 10.1039/c6lc00840b

www.rsc.org/loc

Electroporation has been one of the most popular non-viral technologies for cell transfection. However, conventional bulk electroporation (BEP) shows significant limitations in efficiency, cell viability and transfection uniformity. Recent advances in microscale-electroporation (MEP) resulted in improved cell viability. Further miniaturization of the electroporation system (*i.e.*, nanoscale) has brought up many unique advantages, including negligible cell damage and dosage control capabilities with single-cell resolution, which has enabled more translational applications. In this review, we give an insight into the fundamental and technical aspects of micro- and nanoscale/nanochannel electroporation (NEP) and go over several examples of MEP/NEP-based cutting-edge research, including gene editing, adoptive immunotherapy, and cellular reprogramming. The challenges and opportunities of advanced electroporation technologies are also discussed.

1. Introduction

Electroporation is one of the most commonly used methods for non-viral gene delivery. It has played a particularly important role in recent breakthroughs in life sciences, such as gene editing (*e.g.* CRISPR-Cas9),[1–3] adoptive immunotherapy (*e.g.* chimeric antigen receptors (CARs)),[4] and cell reprogramming (induced neurons (iNs)).[5,6] Non-viral approaches are typically classified into two categories, chemical and physical methods. Chemical methods include nanocarriers (*e.g.* lipoplex, polyplex), where cargo is intracellularly delivered through endocytosis followed by endosomal escape. These methods, however, tend to be slow and relatively inefficient.[7] Physical methods (*e.g.*, electroporation), on the other hand, are more straightforward and simpler to implement, as the cells can be directly permeabilized with a specific stimuli (*e.g.*, mechanical, electrical, optical, *etc.*), which facilitates entry of "naked" cargo (*e.g.*, DNA, RNA, proteins, *etc.*) into the cells.[8]

Bulk electroporation (BEP) is a commercially available and affordable technology with a relatively simple setup, where the cells and cargo are first loaded into a dielectric chamber upon which a bias (typically >1000 volts) is applied, thus causing membrane poration and diffusion/endocytosis-based cytosolic cargo delivery. Nevertheless, despite its simplicity, BEP-mediated transfection causes multiple adverse side effects, including pH changes and significant joule heating, which markedly hamper cell viability, especially in primary cell cultures.[9]

Microscale electroporation (MEP) systems, which were introduced in the early 2000s,[10] use a microelectrode setup that allows for the implementation of stronger and more uniform porating electric fields at significantly lower voltages compared to BEP, thus minimizing cell death. Nevertheless, like in BEP, cytosolic cargo delivery is regulated by diffusion and endocytosis-like processes, whose efficiency is considerably limited by the cargo size.

In contrast, nanoscale- or nanochannel-based electroporation (NEP) is a novel single-cell resolution transfection approach in which strong but nanoscale focused electric fields result in transfection efficiencies and cell viabilities of nearly 100%. Moreover, unlike BEP or MEP, cytosolic cargo delivery is modulated by electrophoresis, thus enabling dosage control capabilities not seen with any currently available transfection technology.[11]

A number of reviews have addressed BEP- or MEP-based transfection systems.[9,10,12,13] Recently, we briefly touched upon a few emerging nanotechnologies for electroporation applications.[14] Here we will focus, among other things, on the research and design (R&D) efforts conducted to transition from BEP/MEP to NEP. We first describe the fundamental

[a] *Department of Biomedical Engineering, The Ohio State University, Columbus, OH, 43210, USA. E-mail: lee.31@osu.edu, gallegoperez.1@osu.edu*
[b] *School of Mechanical and Materials Engineering, Washington State University, Pullman, WA, 99164, USA*
[c] *Department of Mechanical and Aerospace Engineering, The Ohio State University, Columbus, OH, 43210, USA*
[d] *William G. Lowrie Department of Chemical and Biomolecular Engineering, The Ohio State University, Columbus, OH 43209, USA*
[e] *Department of Electrical and Computer Engineering, The Ohio State University, Columbus, OH 43209, USA*
[f] *Department of Surgery, The Ohio State University, Columbus, OH 43210, USA*
† These authors contributed equally.

aspects and practical issues of BEP that led to the development of the MEP technology. Two major prototypes of MEP, including micro-electrode- and microfluidic-based electroporation, are briefly discussed. Finally, the recent applications of MEP and in particular NEP in cell transfection are summarized. The scenarios of using advanced electroporation devices for non-viral adoptive immunotherapy, gene editing, regenerative medicine and intracellular gene interrogation will be especially highlighted.

2. Miniaturization of electroporation

2.1 Conventional electroporation

Electroporation-based gene delivery was first reported back in 1982,[15] and since then numerous studies have used this approach to introduce exogenous cargo into cells both *in vitro* and *in vivo*. Most electroporation experiments are conducted in millimeter- to centimeter-sized chambers.[16] Fig. 1 shows a typical setup of a BEP system. A high voltage is applied across parallelly or coaxially arrayed electrodes immersed into the chamber within the mixture of cells and exogenous cargo. This results in the formation of a transmembrane potential (Δ_m) across the lipid bilayer. Once Δ_m reaches a critical value, the lipid molecules within the membrane rearrange to form small openings on the cell membrane that facilitate cargo translocation into the intracellular space through diffusion/endocytosis.[17] A major advantage of the BEP approach is its ability to handle millions of cells. BEP-based systems have been extensively discussed in the literature.[17–26] Here we will discuss some fundamental aspects and considerations of the BEP process.

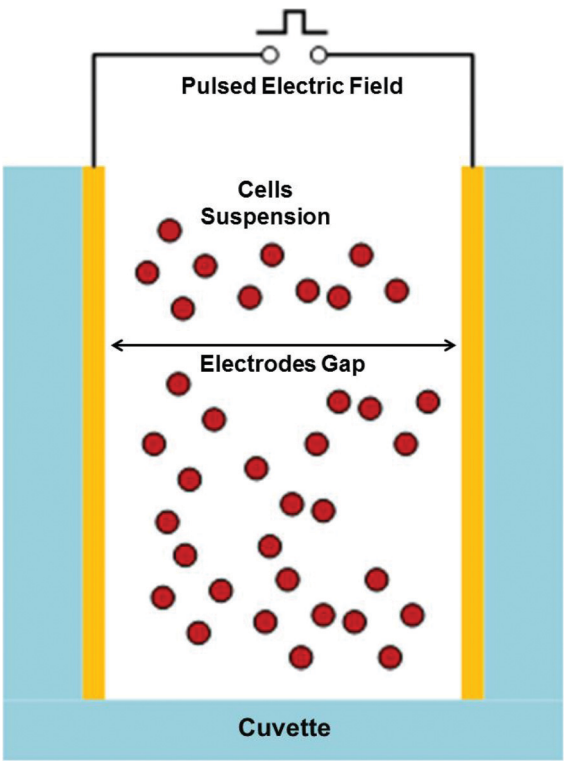

Fig. 1 Schematic of a bulk electroporation system. The electrode gap is larger than the size of a single cell by several orders of magnitude.

2.2 Mechanism and models of BEP

Although multiple studies have looked into the process of membrane electroporation ever since the first study on electropermeabilization was published in 1958,[27] the underlying modulating mechanisms have not been fully elucidated yet, in part because of the lack of tools with high enough resolution to document the process in real time.[18,23] A number of theoretical models on Δ_m and the process of membrane breakdown have been postulated; however, proper experimental validation of every single detail remains challenging.

BEP can be broken down into six stages: (i) application of a pulsed high voltage (around 1 kV cm^{-1}) to the electrodes; (ii) accumulation of positive and negative charges on the cell membrane; (iii) rearrangement of the lipid molecules on the cell membrane once Δ_m reaches a critical value; (iv) nanopore formation on the cell membrane (*i.e.*, aqueous pathways); (v) intracellular cargo translocation mostly by diffusion/endocytosis-based processes; and (vi) membrane repair (*i.e.*, reversible electroporation or RE). However, oftentimes, high electric fields could cause irreversible electroporation (IRE), which is known to result in cell lysis and death.[28,29]

In BEP, size disparities between the electrodes, chamber and cells lead to non-uniformly distributed electric fields at the single cell level. Different models have thus been developed for Δ_m under low cell densities.[17–19,23–25] An example is shown in eqn (1):

$$\Delta_m = -f \cdot E \cdot R \cos\theta \cdot \left(1 - e^{-\frac{t}{\tau}}\right) \quad (1)$$

where f is the form factor related to the shape of the cell, E is the external electric field, R is the radius of the cell, θ is the polar angle between the direction of E and a given point on the cell membrane, t is the lasting time of E, and τ is the time constant of the cell membrane. In most cases, the transient terms in eqn (1) can be ignored as the cell membrane charging time is significantly shorter than the pulse duration ($\tau \ll t$, the pulse duration[23]); therefore, eqn (1) can be simplified as:

$$\Delta_m = f \cdot E \cdot R \cdot \cos\theta \quad (2)$$

Eqn (2) is referred to as the steady-state Schwan equation.[18] The form factor f is 1.5 for spherical cells and 0.5 for elongated cells.[23] Eqn (2) is commonly used to calculate Δ_m for a limited number of cellular shapes and densities. Recently, finite element methods (FEMs) were used to calculate the electric field distribution and Δ_m on single cells with irregular shapes or high cell densities.[18]

As discussed previously, membrane poration occurs when Δ_m reaches a critical value (Δ_s) of approximately 0.5–1 V.[17] Poration and diffusion/electrophoresis-based cargo translocation

can be described by eqn (3):[18]

$$\frac{V}{S_p}\frac{dc}{dt} = -D\frac{zEF}{\rho T}c - D\nabla c \quad (3)$$

where V is the cell volume, S_p is the surface area of the permeabilized cell membrane, c is the concentration of the cargo transported across the cell membrane, and D is the diffusion coefficient. The first term on the right side of eqn (3) describes the electrophoretic component of the process, which is dependent on the electrical charge (z) of the molecules and the local electric field (E). The second term is the diffusion component, which is driven by the concentration difference (∇c) across the cell membrane. Electrophoresis is believed to be the dominant factor while the electrical stimulation is applied. Diffusion plays a more prominent role when the external electric field is turned off. It is believed that a small cargo and ions transport across the cell membrane through diffusion, while a large cargo (*e.g.* plasmids, proteins, *etc.*) mainly depend on electrophoresis.

2.3 BEP setup

Commercially available BEP systems consist of a cuvette with built-in electrodes and power supply for pulsed voltage generation (*e.g.* Lonza Nucleofector™, Lonza Group, US). For *in vivo* applications, needle electrodes are usually used to penetrate tissues (*e.g.* NEPA21, NEPA gene, Japan). Various approaches have been reported to enhance the performance of BEP. Zu *et al.* added gold nanoparticles (AuNPs) in the cell buffer and demonstrated that the transfection efficiency can be improved 2–3-fold without compromising cell viability.[30] Zhao *et al.* recently developed a flow-through BEP device.[31] Cells flow through a large tube (inner diameter, 6.8 mm) at a high rate (2×10^7 cells per min). Three groups of needle electrode arrays (0.3 mm diameter, 1 mm center to center distance) were built-in the tube. Square wave pulses were then sequentially applied on 2 of these 3 groups each time to achieve a more uniform electric field distribution. This configuration resulted in 60% transfection efficiency and 80% cell viability.[31]

2.4 BEP considerations

BEP has been used to deliver a wide variety of cargo, including nucleic acids, to proteins, enzymes, and antibodies.[32–34] Recent studies, for example, have used BEP-based delivery of Cas9 protein for gene editing purposes.[6,13,35] Although BEP-based systems show multiple practical advantages, including (1) well-established protocols, (2) user-friendliness, and (3) high-throughput transfection, the high voltage (>1000 V) requirement continues to be a significant limitation. Eqn (2) implies that an electric field as high as 1.3 kV cm^{-1} is needed in order to achieve a 1 V Δ_m on a spherical cell with a radius of 5 μm. If the gap between the electrodes is set to about 5 mm (typical in BEP), a bias of 650 V or higher needs to be applied to the cell/cargo mixture. Such a high voltage tends to cause a significant decrease in cell viability due to joule heating, pH changes, and bubble formation. Moreover, typical BEP experiments handle large cell numbers per transfection, which results in randomly distributed electric fields and Δ_m (at the single cell level). This in turn could lead to highly stochastic transfection profiles and cell lysis in most cases. Such stochasticity can be further exacerbated by the diffusion-based cargo uptake process.

3. Microscale electroporation

MEP-based systems emerged as a more benign and controllable alternative to BEP-based transfection. The first flow-through MEP device was made of a micro-machined poly(methyl methacrylate) (PMMA) chip, which consisted of a 0.2 mm × 5 mm × 25 mm channel and gold electrodes coated on both top and bottom surfaces using thermal evaporation.[36] Subsequent studies resulted in the development of many MEP-based systems.[10,16,37–43]

3.1 MEP setup

Rubinsky and colleagues were among the first to study single-cell electroporation on a microhole chip,[25,44,45] which allowed direct monitoring of the electrical current and associated membrane breakdown. Lin's group developed the first flow-through microfluidic device for cell electroporation in 2001.[36] Currently available MEP devices are mainly based on these two prototypes, namely (i) micro-electrode electroporation (MEEP) and (ii) flow-through microfluidic electroporation (MFEP). MEEP typically requires single-cell entrapment within a microelectrode system before the porating electric field is applied. In contrast, MFEP is based on a process where cells are continuously flowing thorough a pair of electrodes within a microfluidic channel where the porating field is applied.

MEEP can be further divided into two subgroups, *i.e.* localized MEEP and random MEEP. In random MEEP, tens to hundreds of cells are loaded into a micro-scale cuvette (~100 μm in width) and electroporated with embedded patterned microelectrodes.[46,47] Liang's group developed a high-throughput MEP chip for siRNA delivery.[46] In this case, cells are loaded into arrays of millimeter-scale wells, which are then electroporated using patterned spiral microelectrodes (Fig. 2A and B).[46] Numerical simulations show that an applied bias of 150 V is sufficient to generate a uniform electric field of 300 V cm^{-1}. This MEP device design was reported to achieve transfection efficiencies and cell viabilities of around 90% and 80%, respectively. However, stochastic cell transfection[46] and localized cell death (Fig. 2C–E) remain challenges with this type of systems.[47–51]

Localized MEEP appears to offer additional advantages. In localized MEEPs, a micro-electrode[25,44–46,52–55] or micro-electrode array,[56–60] with dimensions smaller than the cell, are manufactured in the form of micro-needles and spikes or patterned in microholes/nozzles/channels, *etc.* Highly localized electric fields are generated over a single cell or several

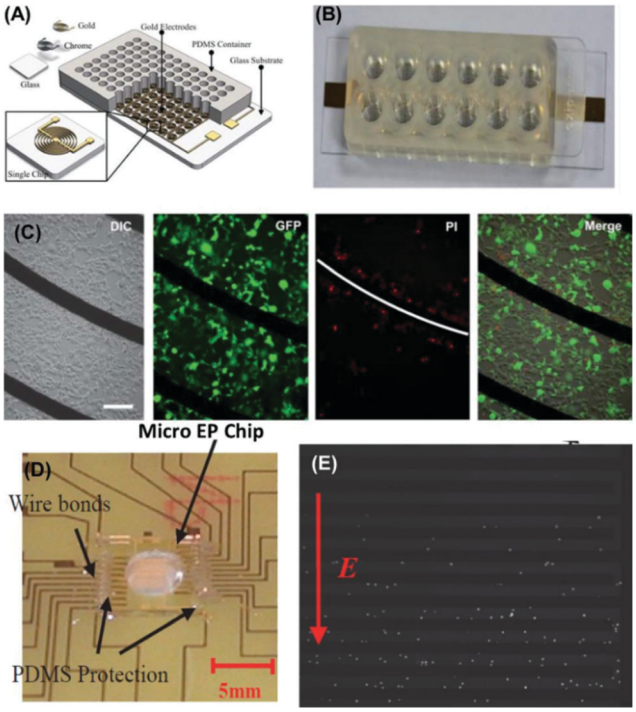

Fig. 2 Schematics and experimental setup of micro-electrode electroporation (MEEP) devices for high-throughput cell transfection. (A) Schematic diagram of the spiral-shaped micro-electrodes. (B) Assembled 12-well MEEP device. (C) Differential interference contrast (DIC) and GFP fluorescence images show the cells transfected with GFP plasmids. PI dye staining indicates dead cells after electroporation.[46] Reproduced with permission from RSC. (D) A micro-electroporation chip that can process thousands of cells simultaneously. (E) Fluorescence images show a gradient of transfection efficiency related to the electric field strength by using this chip.[47] Reproduced with permission from IEEE.

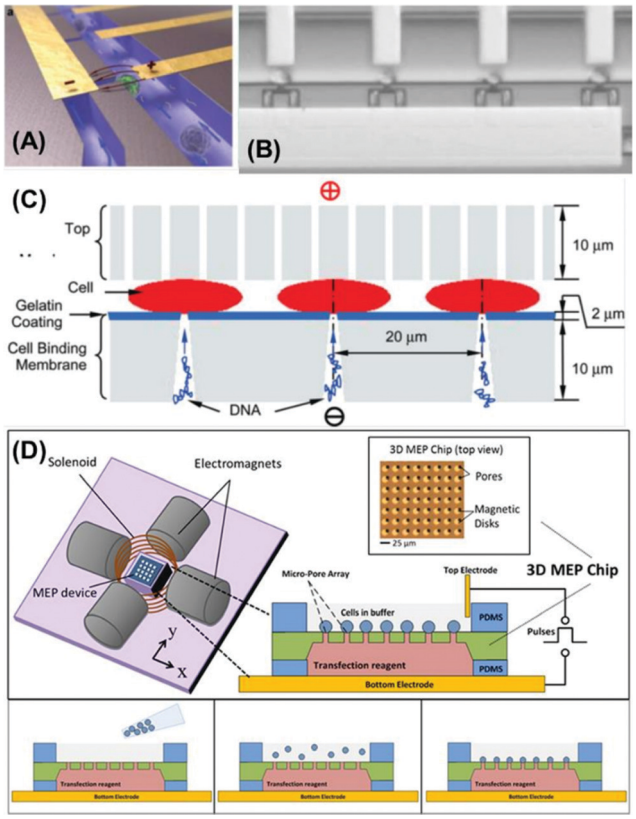

Fig. 3 Representative micro-electrode array chips for localized and high-throughput cell electroporation. (A and B) Microfluidic MEEP devices for single-cell electroporation.[56] Reproduced from ref. 54 with permission from RSC. (C) Micro-nozzle-based MEEP system.[58] Reproduced with permission from ACS. (D) Magnetic tweezers-based MEP platform.[61] Reproduced with permission from Wiley.

cells so that the electric field can be intensified by 2–3 orders of magnitude. A low-voltage (*e.g.*, <5 V) is sufficient for cell permeabilization under this configuration. The first attempts at localized MEEP focused on placing a micro-electrode, which could be carbon fiber-based[54] or an electrolyte-filled capillary,[52,55] within 10 μm of the cell to be transfected. Subsequent modifications were introduced to MEEP systems using microfabricated systems that enabled cell alignment with the applied electric field[44] and high-throughout transfection.[57] Valero *et al.* developed a device that could independently electroporate 9 cells by positioning them to 9 microholes in between two parallel channels (Fig. 3A and B).[56] Cells are trapped towards the microholes by generating a pressure difference between two parallel channels, which essentially concentrated the electric fields at the microholes. With this configuration, biased voltage of <4 V successfully transfected the cells. Transfection efficiencies and cell viabilities hover around 75% and ~100%, respectively. We developed a sandwich-type MEEP for high-throughput transfection of mouse embryonic stem cells[58] (Fig. 3C).

Cells were sandwiched between two gelatin-coated polyethylene terephthalate (PET) membranes. The bottom membrane had an array of micromachined nozzles (2.5 μm in diameter), and the top membrane had track-etched pores of 1 μm. Vacuum was applied through the bottom membrane to trap each cell on a nozzle. This was then followed by the implementation of a voltage across the sandwich system to (i) localize the porating electric field on single cells, and (ii) electrophoretically drive negatively charged cargo (*e.g.*, DNA) through each nozzle into the cytosol. Electrophoresis-driven cargo delivery in this system, however, is limited, given the fact that the applied voltage cannot exceed 20 V to avoid cell lysis.[58] In order to minimize cell damage due to vacuum forces and/or hydrodynamic cell trapping, we developed a magnetic tweezers-assisted MEEP platform[61] (Fig. 3D), where cells tethered with magnetic beads can be precisely positioned over porating silicon-based microchannels *via* remote control. Such a system was successfully used to transfect large cell numbers (approximately 40 000 cells per cm^2) with high efficiency. Additional magnetic tweezers-based systems have been reported in the literature as well.[62]

MFEP-based approaches, on the other hand, transfect cells as they flow through microchannels. Porating voltages are typically applied through needle electrodes inserted into the microchannels. Recent studies, however, have used

electrodes that have been directly patterned on the microchannel(s) surface. MFEP systems tend to be easier to manufacture compared to MEEP, especially considering recent advances in microfluidic technologies, and have the potential to handle a larger number of cells over the long run.[36,63–79] Successful MFEP-based transfection requires precise synchronization between the flow rate and the implementation of the porating bias. Some studies have addressed this requirement by focusing the porating electric field, often based on direct current, on a narrow portion of the microfluidic channel where only single cells can flow through.[64,67,72,76] MFEP devices have been reported to handle approximately 10^4–10^8 cells per minute.[73] Different permutations of MFEP-based approaches have also been reported, including one in which single cells are transfected within oil phase droplets at relatively low voltages (4–7 V) with reported transfection efficiencies and cell viabilities of 11% and 20%, respectively (Fig. 4A).[63]

Zhu *et al.* introduced a hydrodynamic focusing electroporation device in which cells were sandwiched/transfected between two conductive fluid flows (Fig. 4B).[77] This system reported transfection efficiencies and cell viabilities of 70% and 30%, respectively. Wei *et al.* developed a laminar flow electroporation platform that used hydrodynamic focusing to generate a buffer layer to help protect the cells from excessive electrode/solution heating, electrolysis and bubble formation (Fig. 4C).[78] This device could achieve a 90% transfection efficiency with 60% cell viability.[78] Lu's group pioneered the development of advanced MFEP systems[80–83] for different applications, including gene delivery,[84–86] intracellular molecular tracking,[87,88] and cell sampling.[89,90] Recently, a vortex-based MFEP system was developed to apply hydrodynamic forces and controllably rotate the cells for more uniform membrane poration (Fig. 4D).[74] In another report, a PDMS-based MFEP system, with dimensions of 150 μm × 40 μm × 3.8 mm, was devised to investigate the dynamics of protein delivery into mouse embryonic fibroblasts[88] using a cyan/yellow fluorescent protein pair (ECFP/YPet) as model cargo. Results indicated that successful cargo translocation increased in direct proportion to the electric field, while cell viability decreased significantly at higher fields.

In addition to delivering conventional cargo such as genes and drugs, MFEP has also been used for direct delivery of proteins,[40,68,91] which offers some advantages compared to plasmid gene delivery, including faster action and enhanced ability to control the effective dosage.

In MFEP, the electrodes can be easily configured in different manners within the microfluidic device, including same patterning side[47,63,68,71,92] (Fig. 5A[68]) or opposite sides (Fig. 5B[36] and C[70]), with leads extending out of the microfluidic outlet/inlets[64,67,69] (Fig. 5D[67]). The electrodes at the same time can be of different shapes, such as stripes,[63] sawtooth,[70] comb,[68] parallel plate,[36] curved stripe,[46] and needle.[67] There are no restrictions on the design, dimension shapes and arrangement, and as such, the electrical field distribution and electroporation performance vary significantly from design to design.

3.2 Theoretical analysis of MEP

The major differences between MEP- and BEP-based systems stem from how the porating electric field is applied. In MEP, system miniaturization results in more localized/enhanced implementation of the electric field on individual cells, which results in successful transfection at relatively low voltages (*e.g.*, 1 V for MEP *vs.* >1000 V for BEP) and improved cell viability and transfection efficiencies. Moreover, MEP-based

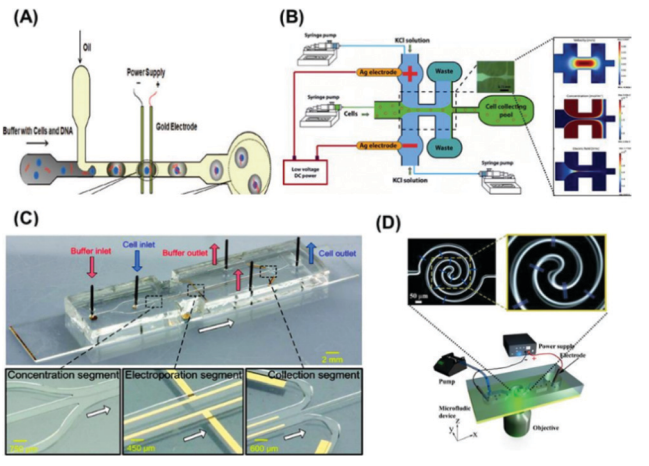

Fig. 4 MFEP-based approaches for continuous cell transfection based on a variety of designs. (A) Droplet encapsulation,[63] (B) hydrodynamic focusing,[77] (C) laminar flow electroporation[78] and (D) vortex-assisted microfluidic device.[74] Reproduced with permission from ACS, Springer, ACS, and RSC, respectively.

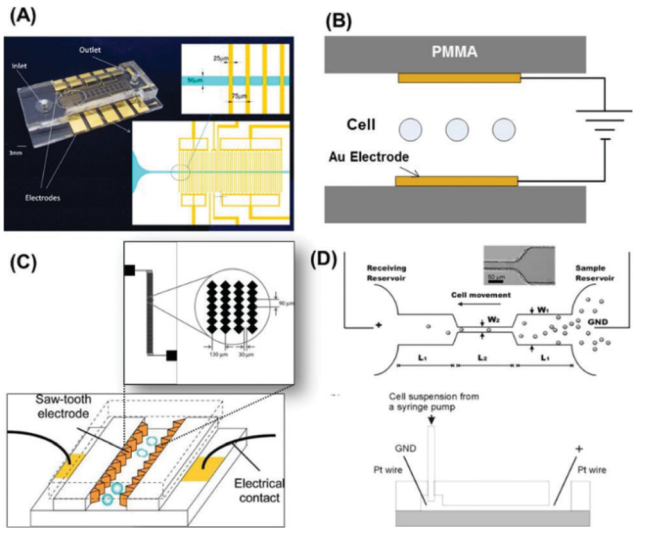

Fig. 5 MFEP devices with different designs of the electrodes, including (A) comb-shaped electrodes patterned on one side of a microchannel,[68] (B) parallel electrodes fabricated on both sides,[36] (C) sawtooth electrodes on both sides of a microfluidic channel,[70] and (D) needle-type electrodes placed on the terminals.[67] Reproduced with permission from ACS, Elsevier, RSC and ACS, respectively.

systems tend to allow concomitant *in situ* cell monitoring and can also be interfaced with multiple systems to enable the development of advanced biointerrogation/manipulation platforms.

Multiple simulation studies have been conducted on MEP-based processes.[47,93–95] FEM studies conducted by Movahed and Li on a particular MEP configuration (5–20 μm electrodes embedded within a 25–30 μm deep microchannel, and a 30 μm diameter cell) show that voltages between 1 and 3 V would result in successful membrane permeabilization around the cell poles (opposite to the embedded electrodes). Pore formation (*i.e.*, size and density) could conceivably be controlled by adjusting the electric field intensity.

Kaner *et al.* investigated how the electrode configuration influenced electric field distribution and membrane permeabilization within a microfluidic channel.[94] The results showed that the permeabilized cell hemisphere is determined by the electrode location, with a single hemisphere/pole permeabilizing when both electrodes are on the same side of the microchannel *vs.* both hemispheres and poles when the electrodes are on opposite sides (Fig. 6A and B).[17,94] The permeabilization extent was also predicted to be a function of the applied voltage (Fig. 6C).

As discussed above, the electrode/cell configuration plays a major role in determining the outcome of MEP-based processes. Such configuration is fundamentally different in MEEP *vs.* MFEP systems, with MEEP devices typically allowing closer contact between the cell and the electrode system. An example of this is shown in Fig. 7A.[57] FEM analysis of this system indicated that the porating electric field mainly focused on the portion of the cell that is inside the microchannel (Fig. 7B).[57] Fei *et al.* developed a micro-nozzle-based MEP platform where electric field focusing occurs mostly around the converging nozzle areas (Fig. 7C). Such a shape is also expected to enhance electrophoresis-mediated cargo delivery.[58] Studies by Ionescu-Zanetti *et al.* found that electrophoresis could significantly reduce the time needed for successful cargo delivery into the cell.[60]

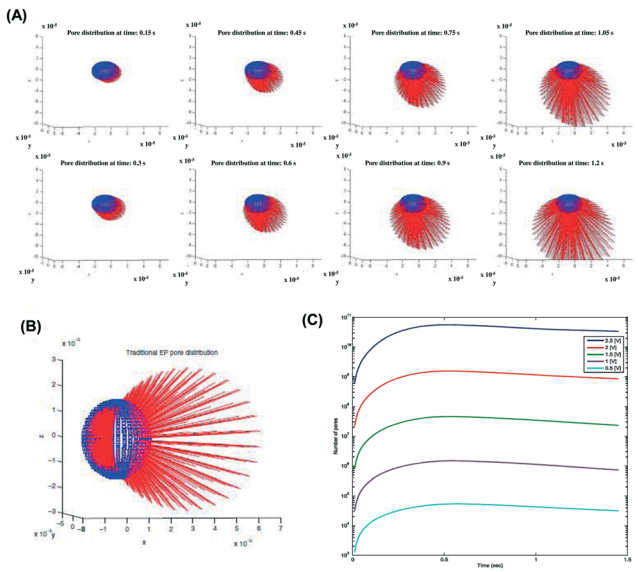

Fig. 6 Numerical simulations of single cell electroporation in MEP devices. (A) Radiation-plots show that the formed nanopores are mainly distributed on the bottom hemisphere of the cell when both electrodes are placed on the bottom side of the microchannel. In contrast, (B) the nanopore distribution becomes more homogeneous when the electrodes are on both sides.[94] (C) FEM simulation shows the number of nanopores formed on the cells as a function of the applied voltage and the time.[94] Reproduced with permission from Springer.

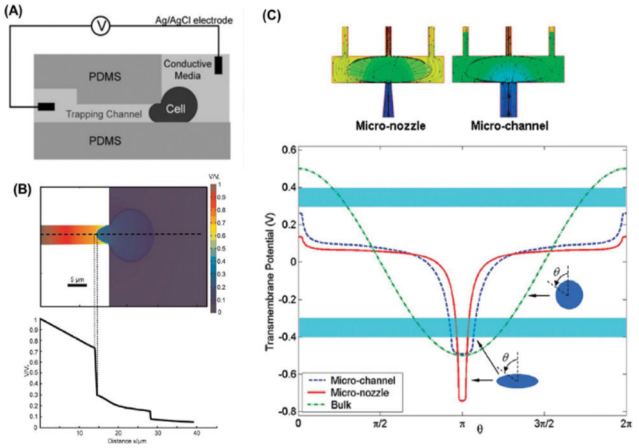

Fig. 7 MEEP-based systems and electric field distribution. (A) Schematic of a single cell trapped into a microchannel, which leads to (B) highly localized electroporation and the concentration of the potential drop on the cell membrane within the microchannel.[57] Reproduced with permission from RSC. (C) Electric field distribution for the micronozzle array.[58] Reproduced with permission from ACS.

Finally, joule heating and pH changes could significantly alter the outcome of MEP-based experiments.[72] For example, studies using temperature sensitive dyes (Rhodamine B) in MFEP devices showed that under a high electric field (800 V cm^{-1}) and with a low flow rate (<2.13 μL min^{-1}) the local temperature could reach cytotoxic levels of up to 45 °C. Other groups studied the effects of pH changes in cell viability,[48] and they found that the pH values could range between 3 and 10 around the anode and cathode, respectively, with cells near the electrodes being more susceptible to death.[48]

4. Nanoscale electroporation systems

Further miniaturization of the electroporation systems has enabled advanced functionalities compared to BEP- or MEP-based setups. Nano-electroporation (NEP) systems, for example, focus the porating electric field on a considerably smaller (*i.e.*, nanosized) portion of the cell membrane, which results in the development of a much larger Δ_m while causing minimum to negligible damage to the cell. Here we will go over a number of representative NEP-type systems and discuss manufacturing, theoretical and experimental aspects.

4.1 NEP-based systems

A number of NEP-based systems have been developed over the years, including (i) two-dimensional (2D) nano-channel

electroporation,[96–98] (ii) nano-straw/nano-spike electroporation,[99–101] (iii) nano-wire/nano-electrode electroporation,[102–104] (iv) nano-probe (or nanofountain-probe) electroporation,[105,106] and (v) three-dimensional (3D) nano-channel electroporation.[107] Our lab was the first to develop an NEP-based system for efficient cell transfection.[96] The basic functional unit of this first generation device consisted of a nanochannel (90 nm in diameter, 3 μm long) interconnecting two microchannels (Fig. 8). These devices were fabricated through a simple replica molding process from lithographically fabricated polydimethylsiloxane (PDMS) masters with stretched/combed DNA strands that ultimately gave rise to the nanochannels (Fig. 8A).[96] Single cells were then loaded into each microchannel, in close contact with the nanochannel output, while the juxtaposing microchannel was filled with the cargo (*e.g.*, DNA, RNA, *etc.*) solution to be delivered (Fig. 8B).[96] A pulsed electric field (150–350 V, 2–10 ms pulses) was subsequently applied across the nanochannel, which induced nanoscale-sized membrane permeabilization immediately followed by electrophoretic cargo delivery into the cytosol. Single-cell resolution dose control could be achieved by modulating the pulse length.

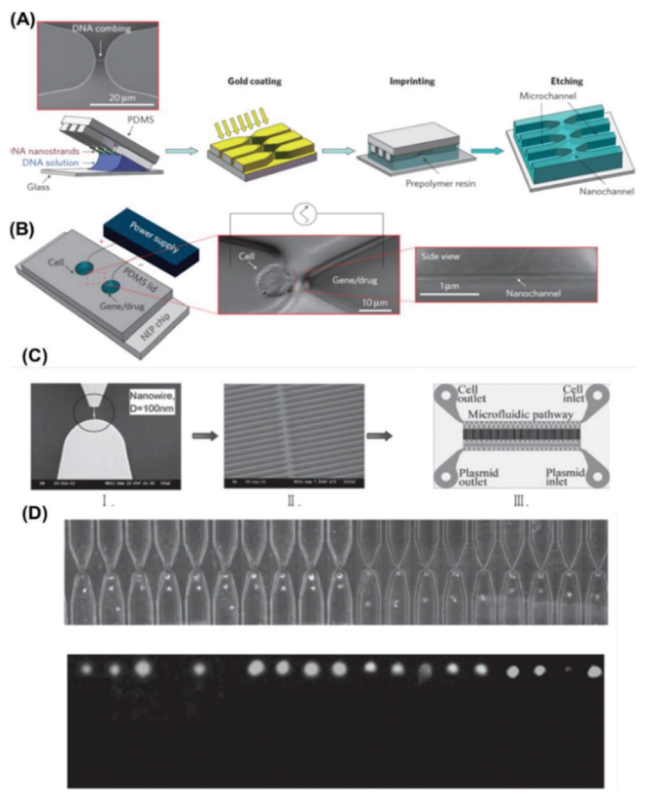

Fig. 8 2D NEP. (A) Fabrication process of NEP devices. (B) Assembly and operation of 2D NEP devices. Single cells were precisely positioned against the nanochannel outlet *via* optical tweezers.[96] (C) PDMS/DNA master and replica-molded device. (D) Cells loaded into the microchannels before (top) and after (bottom) delivery of OSKM plasmids.[98] Reproduced with permission from Nature and Wiley, respectively.

One unique advantage of NEP-based transfection is that cytosolic cargo delivery is entirely modulated by electrophoretic forces. BEP- or MEP-based approaches are still heavily dependent on downstream processes such as diffusion and/or endocytosis. Electrophoresis-based delivery facilitates the transduction of bulky cargo, such as large polycistronic plasmids encoding for multiple genes (*e.g., Oct4, Sox2, Klf4* and *cMyc* or OSKM). Such a cargo is difficult to deliver using BEP- or MEP-mediated transfection.[98]

The first generation of NEP devices was based on a 2D system with a limited throughput. To increase the yield, we developed 3D NEP systems (Fig. 9) that could simultaneously transfect tens of thousands to hundreds of thousands of cells in a controlled and benign manner.[107] In this case, 3D nanochannel (300–600 nm in diameter, 10 μm long) arrays are created in Si or polymers either by combining projection and contact lithography with deep reactive ion etching (DRIE) (Fig. 9B) or by lithographically patterning a track etched membrane with nanochannels. Such systems can achieve transfection efficiencies and cell viabilities of approximately 90% and 100%, respectively, with minimum cell-to-cell variations in the transfection extent.

Espinosa *et al.* developed a nano-fountain probe electroporation (NFP-E) system for *in situ* cell transfection.[105] This system consists of a hollow atomic force microscopy (AFM) probe with a ~800 nm outlet that modulates membrane poration and cargo delivery (Fig. 10A and B).[105] An automation stage is used to achieve selective single-cell transfection. Moreover, the resolution of the system allows localized transfection of a specific region on the cell. This system, however,

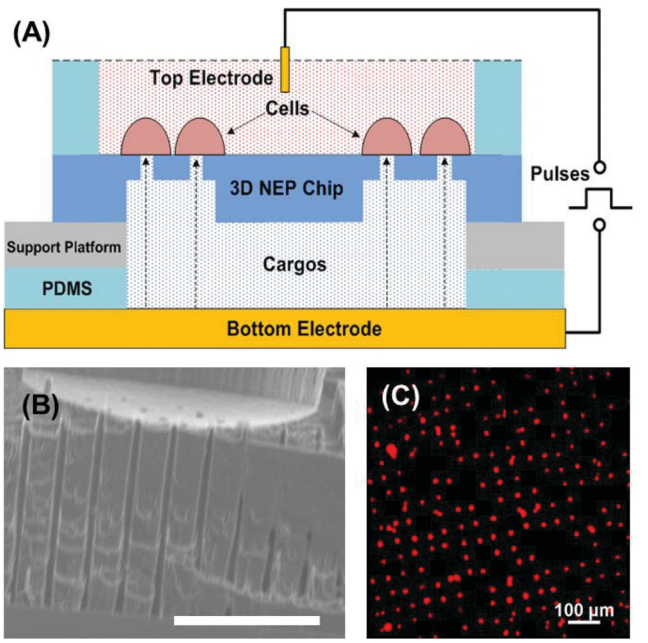

Fig. 9 Si-based 3D NEP platform for high-throughput cell transfection. (A) Schematic of the 3D NEP system.[107] (B) Cross section micrograph. (C) Intracellular fluorescence dye expression after electroinjection through nanochannel array. Reproduced with permission from RSC.

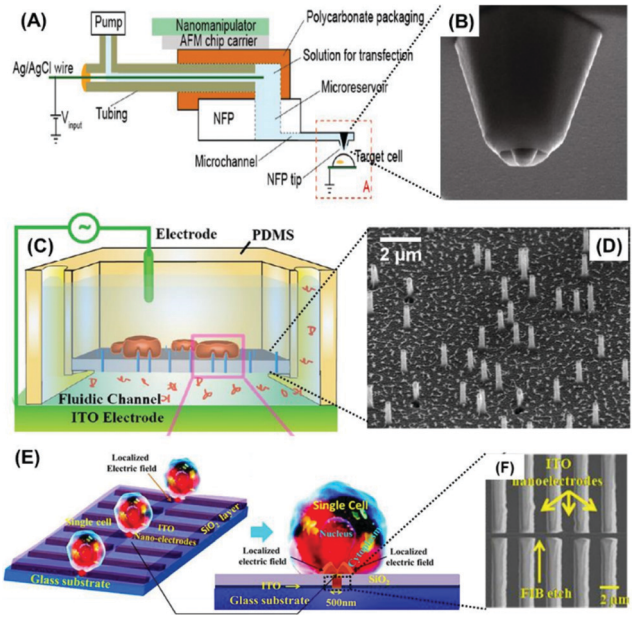

Fig. 10 Additional nanoscale electroporation systems. (A) Schematic and (B) electronic micrograph of the NFP-E platform.[105] Reproduced with permission from ACS. (C) Electroporation-based gene delivery facilitated through (D) nanostraws.[99] Reproduced with permission from ACS. (E) Single cell electroporation by parallel nano-electrodes. (F) Electron micrograph of the ITO nano-electrodes.[104] Reproduced with permission from AIP.

can only handle a limited number of cells. Melosh *et al.*, on the other hand, introduced a novel nanostraw-electroporation platform based on randomly arrayed hollow nanotubes (200 nm in diameter and 1.5 μm in height) (Fig. 10C and D).[99] Such structures were etched out of an alumina coated track-etched polycarbonate membrane to create a direct pathway for the delivery of a wide variety of cargo into cells, with efficiencies ranging between 81% and >90% depending on the cargo. Cellular engulfment of the nanostructures provides tight contact, oftentimes enabling transfection to occur at no or low voltages. By using this nano-fountain probe electroporation system, they have successfully delivered protein and DNA into cells.[89]

In addition to nanochannel-, nanofountain-, or nanostraw-based electroporation, other groups have developed myriads of nanoscale components (*e.g.*, electrodes, nanowires, *etc.*) to further study the electroporation process (Fig. 10E and F) and define optimum voltage and/or frequency ranges to achieve reversible *vs.* irreversible membrane poration.[104]

4.2 Theoretical analysis of NEP

Finite Element Methods has been recently used to study multiple aspects of the NEP process.[96,100,103–105,107] Such models typically represent the cell membrane as a resistor and a capacitor in parallel.[96,105] Once a porating voltage is applied, most of the drop (~95%) occurs across the nanochannel, which has an ohmic resistance value several orders of magnitude higher compared to the cell (*e.g.*, hundreds of MΩ compared to <1 MΩ) (Fig. 8B).[107] As such, the electrical stimuli (Δ_m) modulating membrane poration is mostly focused around the cell-nanochannel outlet interface (within <1 μm, Fig. 11A). Δ_m, at the same time, is extremely sensitive to the gap distance between the cell and the nanochannel outlet, with shorter distances resulting in higher Δ_m values.[96,107]

In addition to promoting highly focused and enhanced Δ_m, nanochannel-based poration also enables fast and efficient direct cargo delivery into the cytosol by electrophoresis. Electrophoretic forces are enhanced within the nanochannel due to the high voltage drop, which allows cargo delivery to occur within microseconds compared to diffusion-dominated processes, which could take a much longer time (*e.g.*, BEP, MEP) (Fig. 11B). Experiments with quantum dots confirmed an electrophoresis-driven speed of about 490 μm ms^{-1} within a nanochannel, which is ~3000 times higher than the velocity within a microchannel-based system.[96]

5. Biomedical applications of micro-/nanoscale electroporation

A number of recent studies have focused on the use of miniaturized (*i.e.*, micro- to nanoscale) electroporation systems for biomedical applications, including adoptive immunotherapy, gene/RNA-based therapies, cell reprogramming, and intracellular biointerrogation of living cells, among others. Electroporation-based methods are compatible with a host of cargo, ranging from genes to proteins or protein complexes, and thus have the potential to enable a multitude of applications. Here we will discuss some of the most relevant breakthroughs in this area.

5.1 Gene therapy

Gene therapy is a simple yet revolutionary concept that seeks to cure or treat diseases by modulating gene expression.[108,109] Multiple clinical trials with improved vector technologies have shown promising results.[109] Current approaches to gene therapy, however, face a number of practical and translational hurdles, including over-dependence on viral vectors and lack of dosage controllability. Deterministic non-viral methods are thus needed to facilitate the transition from the lab bench to the clinic of highly promising gene therapies.[110] Miniaturized electroporation techniques, especially NEP, are poised to significantly impact this field. One area that has attracted a great deal of attention is DNA vaccination, which has been shown to modulate immune responses *via* delivery of plasmid genes that encode for specific antigens.[111] Electroporation-based approaches have been reported to significantly enhance DNA vaccination.[112,113] In this section we will review some of the most relevant studies on the use of miniaturized electroporation approaches for gene therapy.

Adoptive immunotherapy. Therapies aimed at increasing the immune system's ability to combat specific conditions have shown extremely promising results.[114,115] Genetically engineered immune cells (*e.g.*, T cells, NK cells), for example,

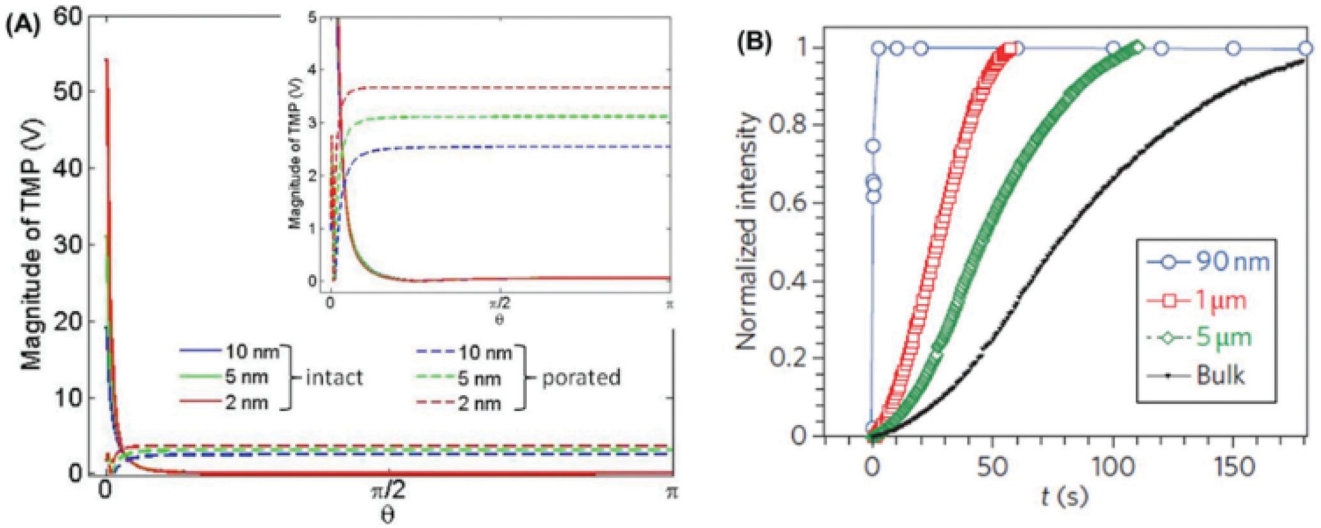

Fig. 11 Numerical simulation of the transmembrane potential and delivery time in NEP (90 nm), BEP and MEP (1 and 5 μm). (A) Transmembrane potential distribution and intensity with respect to the gap distance between the cell and the nanochannel outlet. (B) Delivery time for PI dye in NEP (blue), MEP with 1 μm (red) and 5 μm channel (green), and BEP (black).[96] Reproduced with permission from Nature.

have been used/studied to enhance anti-tumor immunity and vaccine efficacy and to modulate graft-*versus*-host-disease.[103,104,106,116] Nevertheless, immune cell engineering still depends heavily on viral vectors that could hamper clinical implementation. Moreover, immune cells are exceedingly difficult to transfect using conventional non-viral methods such as BEP or nanocarriers.[117–120] We have implemented dielectrophoresis-assisted 3D NEP (pDEP-NEP)[121] platform for non-viral immune cell engineering. Experiments with plasmids encoding for the chimeric antigen receptor (CAR), which has been reported to enhance anti-tumoral activity in immune cells, showed that the pDEP-NEP achieved transfection efficiencies and cell viabilities of around >70% and 90%, respectively (Fig. 12). Conventional BEP, on the other hand, led to transfection efficiencies of <30% and cell viabilities of around 60–70%. In addition, cell-to-cell variability was minimized considerably for pDEP-NEP compared to BEP, which suggests that NEP-based transfection yields more uniformly engineered and possibly predictable/safer cells, which is highly important for clinical translation. Since adoptive

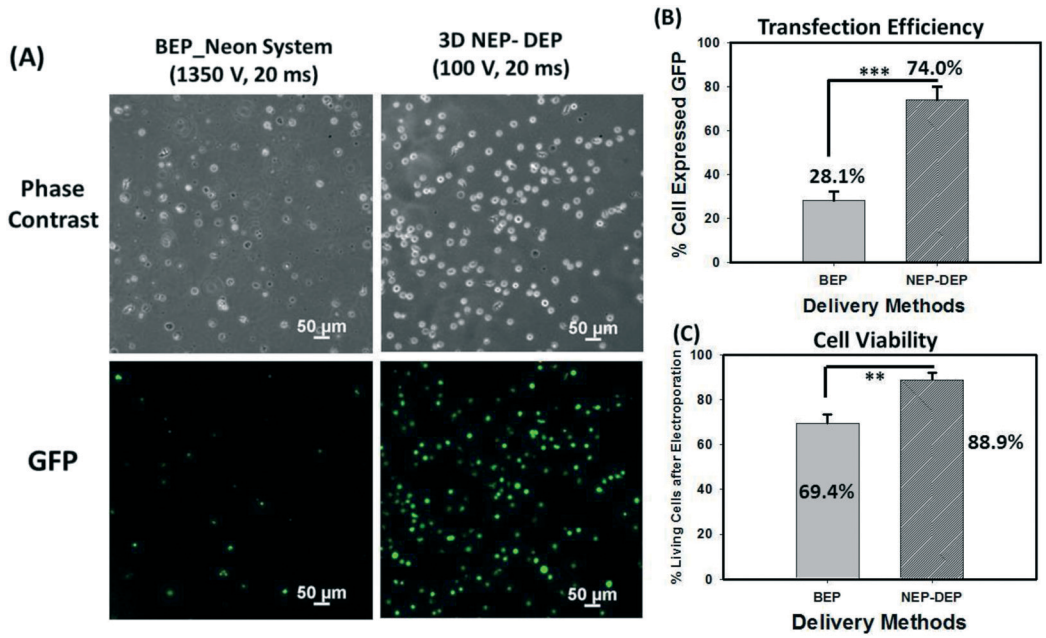

Fig. 12 Safe and efficient NK cell transfection with chimeric antigen receptor (CAR) plasmids by pDEP-NEP.[121] (A) Phase contrast and epifluorescence images of NK cells 10 h after BEP- and NEP-based transfection of CAR plasmids with GFP as reporter gene. Positive epifluorescence signal represents successful expression of CAR gene. (b) Efficiency of CAR plasmid delivery and expression was significantly improved in NEP compared to BEP. ***$p < 0.005$. (C) Cell viability percentages in NEP and BEP. **$p < 0.01$. Reproduced with permission from RSC.

immunotherapy requires permanent transfection of immune cells, the applicability of transient transfection by non-viral methods remains a challenge. Our preliminary data revealed that NEP delivered linear factors was able to provide a longer transfection time than ring-type plasmids delivered by BEP (data not shown). However, more effort is needed in this area.

RNA interference (RNAi)-based therapy. Gene expression for therapeutic applications can also be modulated by transfecting a specific RNAi[122–124] Such a concept has shown great promise for the treatment of a number of diseases, including cancer. Small interfering RNAs (siRNAs) or microRNAs (miRNAs) have been used, for example, to successfully regulate oncogene or proto-oncogene expression (*e.g., VEGF*, *KSP*) in clinical trials for liver cancer.[125] Successful delivery of siRNA or miRNA is the key to efficacious RNAi-based therapeutics.[125] Although nanocarriers have been widely used to deliver RNAis into cells, such an approach presents numerous limitations, including stochastic delivery, size uniformity, aggregation, low loading capacity/efficiency, and poor stability and biocompatibility.[121,126] Recent reports have highlighted the potential of NEP-based transfection for the development of RNAi-assisted therapies. The ability to deliver siRNAs in a dose- and time-controlled manner at the single cell level allowed for the determination of optimum pro-apoptotic strategies for the potential treatment of acute myeloid leukemia (Fig. 13A and B).[127]

Gene editing. Making precise genetic modifications to the living cells has long fascinated bioengineering researchers. Electroporation is found to be frequently utilized in gene editing applications for vector delivery. The CRISPR-Cas9 systems (Clustered Regularly Interspaced Short Palindromic Repeats (CRISPR)—Cas9, a CRISPR-associated protein) recently emerged as a potentially potent genome editing tool in molecular biology. Here we briefly review recent electroporation-involved works associated with the CRISPR/Cas9 gene editing method. Maresch *et al.* demonstrated that by electroporation-based multiplex delivery of CRISPR/Cas9 into mice pancreatic cells, "simultaneous editing" of a number of gene sets in

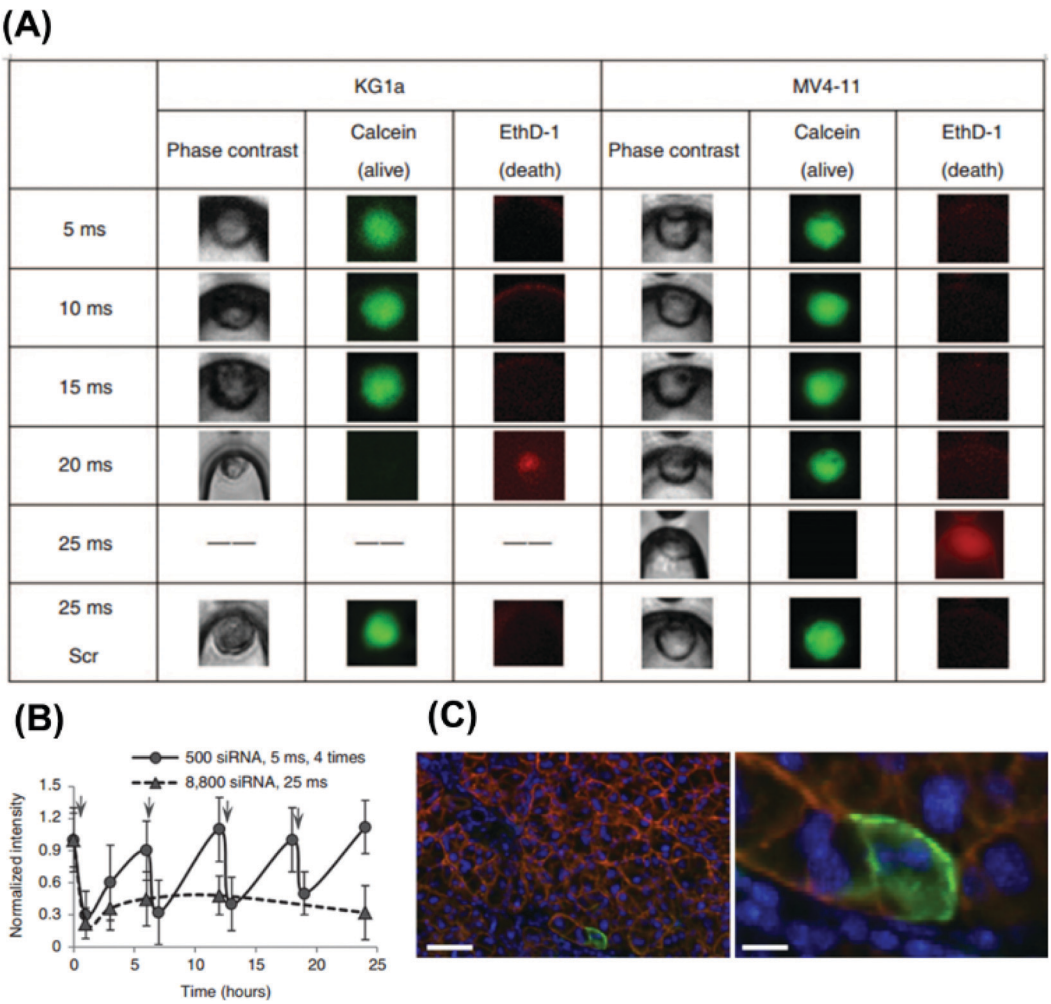

Fig. 13 RNA interference therapy and gene editing. (A) NEP-based *Mcl*-1 siRNA therapy in wild-type and FLT3-ITD AML cells using different NEP conditions. Live/dead cell staining was used to determine the critical dosing to induce cell death. (B) Changes in *Mcl*-1 expression with different siRNA doses.[127] (C) Transition of membranous red to cytoplasmic/membranous green fluorescence in electroporation-transfected acinar cells.[128] Scale bars, 50 μm (left) and 10 μm (right). Reproduced with permission from Wiley and Nature, respectively.

single living cells was realized[128] (Fig. 13C). Their data pointed out that CRISPR/Cas9 will carry out several tasks, ranging from combinatorial gene-network analysis, *in vivo* synthetic lethality screening, to chromosome engineering. Chu *et al.* also presented that enhancing homology-directed repair (HDR) improved the efficiency of CRISPR-Cas9-induced precise gene editing.[129] However, it is worth noting that most of these works pioneering the research of gene editing are heavily dependent on bulk electroporation, which leads to a stochastic and harsh environment to cells *in vivo*. Therefore, it provides great opportunities to MEP and NEP for the study of CRISPR-Cas9 and other gene editing approaches in a more deterministic, real-time and safer manner in the future.

5.2 Regenerative medicine

Many disease conditions are typically caused by quantitative and/or functional deficiencies in specific cell types. The goal of regenerative medicine is thus to replace lost structures and/or functions that result from such deficiencies. Recent advances in nuclear reprogramming (*e.g.*,induced pluripotent

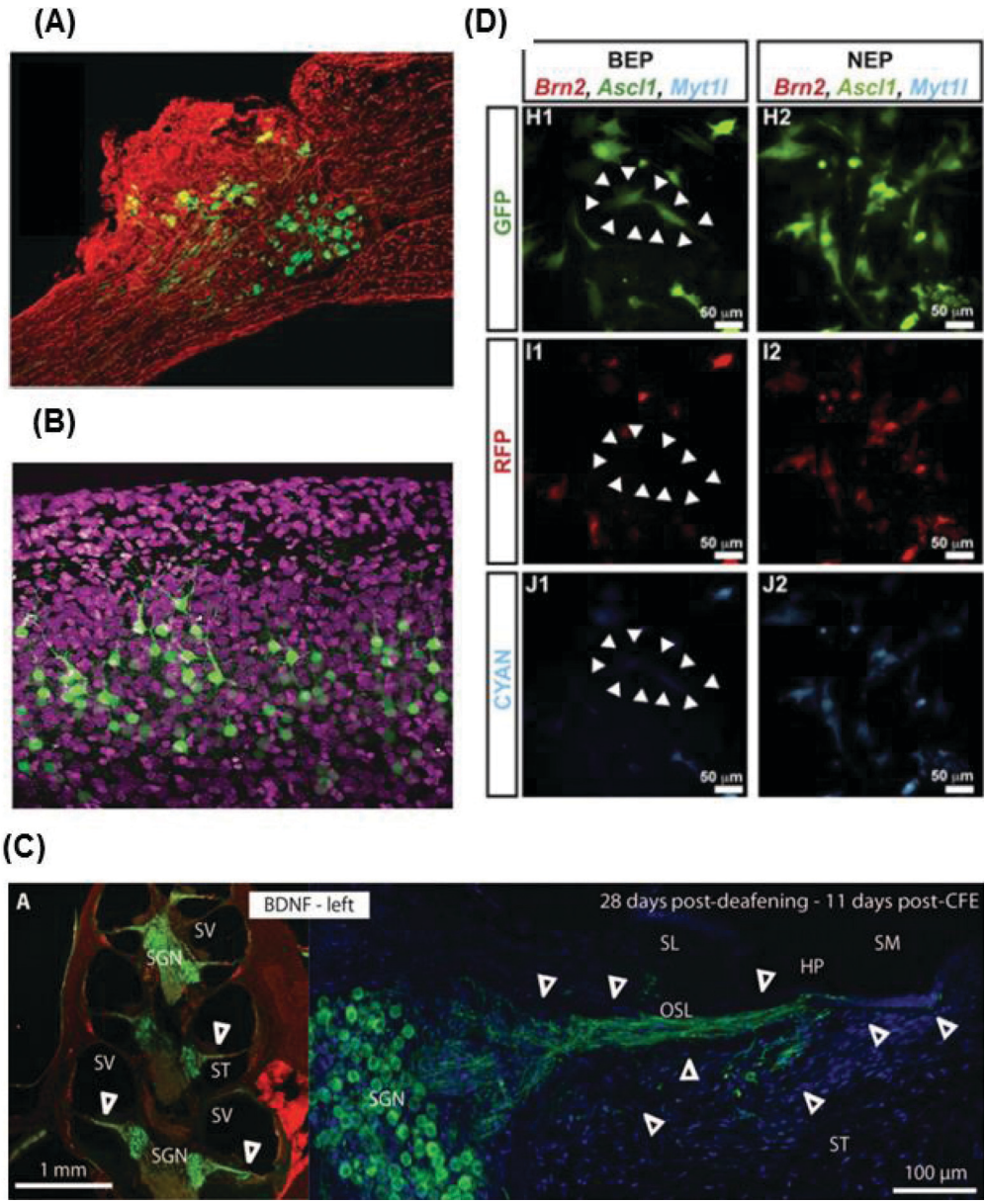

Fig. 14 Recent mice/nanoscale electroporation applications in regenerative medicine. (A) Fluorescence image of an EGFP-transfected dorsal root ganglion (DRG) immunostained with the neuronal marker βIII tubulin (red).[131] Reproduced with permission from Nature. (B) Confocal image of representative electroporated cells (green) from coronal hippocampus. Scale bars, 100 μm.[132] Reproduced with permission from Nature. (C) Representative immunofluorescence image showing that "close-field" electroporation (CFE) mediates BDNF gene therapy in deafened guinea pig cochleae.[133] Reproduced with permission from AAAS. (D) Comparison between BEP- and NEP-based delivery of *Ascl1*, *Brn2*, and *Myt1l* (color coded green, red, and blue, respectively) plasmids into MEFs.[126] Reproduced with permission from Elsevier.

stem cells or iPSCs)[130] have been a great leap forward in regenerative medicine research, especially direct nuclear reprogramming,[118,123] where cells can transdifferentiate directly into the cell of interest without passing through an iPSC stage. Exploiting the full potential of nuclear reprogramming, however, requires precise and timely delivery of complex combinations of reprogramming genes, which cannot be accomplished efficiently with current transfection methodologies due to their highly stochastic nature. The inability to control these factors could lead to inefficient and/or potentially unsafe reprogramming outcomes.

Saijilafu *et al.* presented neuron regeneration work using an efficient *in vivo* electroporation technique enabling accurate and precise manipulation of gene expression.[131] They demonstrated that this method successfully transfected adult dorsal root ganglion (DRG) neurons (Fig. 14A) and thus genetically dissect axon injury and regeneration models. Cancedda's group presented a novel *in utero* electroporation technique based on triple-electrode configuration which firstly transfected Purkinje cells in rat brain areas (Fig. 14B), which had not been achieved before.[132] The *in utero* configuration is promising to provide new insight into neuronal plasticity and can be applied into other tissues including skin and cardiac tissue. Pinyon *et al.* introduced a novel close-field electroporation (CFE) using a cochlear implant electrode, by which for the first time they improved the performance of a "bionic ear" by enhancing the neural interface *via* brain-derived neurotrophic factor (BDNF) delivery (Fig. 14C).[133]

Most of these electroporation devices relied on bulk electroporation. We have developed a novel and yet simple to implement approach to transfect and directly reprogram large numbers of cells in an NEP-like fashion.[126] Deterministic NEP-based delivery of *ABM* (*Ascl1*, *Brn2*, and *Myt1l*) (Fig. 14D) not only resulted in significantly improved reprogramming efficiencies compared to BEP but also allowed us to uncover a number of stochastic barriers to the reprogramming process, including the potential roles of *Ascl1* dosage and the S-phase cyclin CCNA2.

5.3 *In situ* intracellular probing

Disease onset and progression is typically driven by subtle but critical changes in intracellular activity that are often elusive to conventional cell analysis techniques.[129,130,134,135] Novel technologies are thus needed to enable a more thorough monitoring of cellular activity both in real time and at the single cell level.[131,132]

Xie *et al.* developed a vertical nanopillar electroporation device for recording intracellular action potentials in living cardiomyocytes *in vitro* (Fig. 15A).[136] Intracellular recordings were successfully collected on HL-1 cells over a period of four consecutive days (Fig. 15B). Hanson *et al.* used a similar approach to characterize nuclear biomechanics in adherent cells (Fig. 15C).[137] This versatile nanopillar electroporation-recording platform could find applications in drug discovery with electrogenic cells and/or cancer research among other things. Santoro *et al.* carried out a more in-depth study of the interface between 3D nano-electrode structures and cells[138] (Fig. 15D). In addition, a single-cell electroporation and *in situ* recording device has been presented for labeling neurons by Kitamura *et al.*, which enables the recording, labeling and genetic manipulation of single neurons *in vivo* (Fig. 15E).[139]

Zhao *et al.* used 2D NEP to conduct intracellular probing of living AML cells (Fig. 16A) *via* controlled timed delivery of molecular beacons (MBs).[97] Giraldo-Vela *et al.* also used MBs in combination with nanofountain-based electroporation to detect mRNA at the single-cell level (Fig. 16B).[140] Finally, Shalek *et al.* used nanowire-based delivery of siRNAs to conduct *ex vivo* biointerrogation of immune cells (Fig. 16C).[141]

In addition to the biosensors based on nucleic acids, fluorescent biosensors in the form of proteins have also been successfully delivered *via* electroporation.[88] Fluorescence resonance energy transfer (FRET)-based protein biosensors have the potential to monitor the dynamics of protein (*e.g.*, Src)

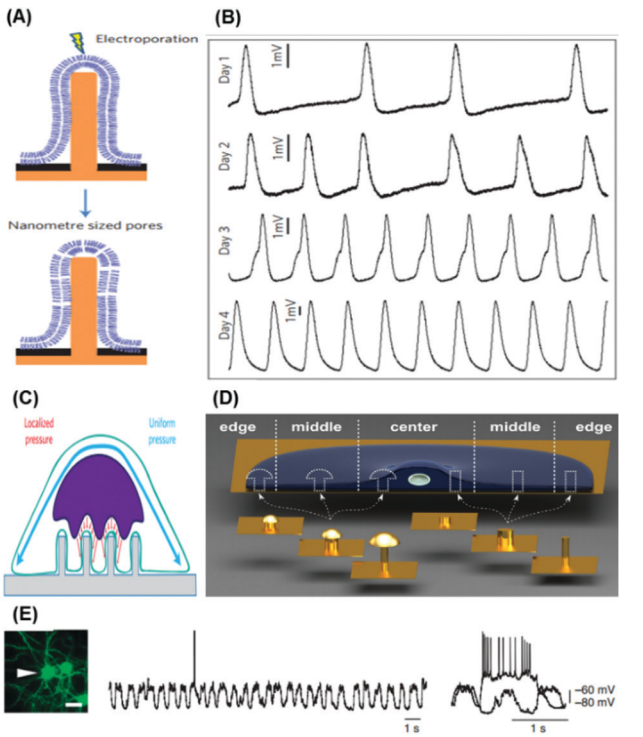

Fig. 15 Electroporation-based intracellular probing. (A) Nanopillar electrode device for intracellular recording of action potentials. (B) Action potentials could be recorded for over four consecutive days at the single cell level.[136] Reproduced with permission from Nature. (C) Vertical nanopillars for probing of nuclear biomechanics.[137] Reproduced with permission from Nature. (D) Schematic diagram illustrating the interface between the nanostructures and cells.[138] Reproduced with permission from ACS. (E) *In vivo* single living cell probe of a neuron 24 h after electroporation. Left: cells with GFP fluorescence were electroporated; the arrowhead indicates the cell recorded. Middle: real-time recording of membrane potential fluctuations and action potentials. Right: responses to current injections of 350 pA and −100 pA. Scale bars, 20 μm.[139] Reproduced with permission from Nature.

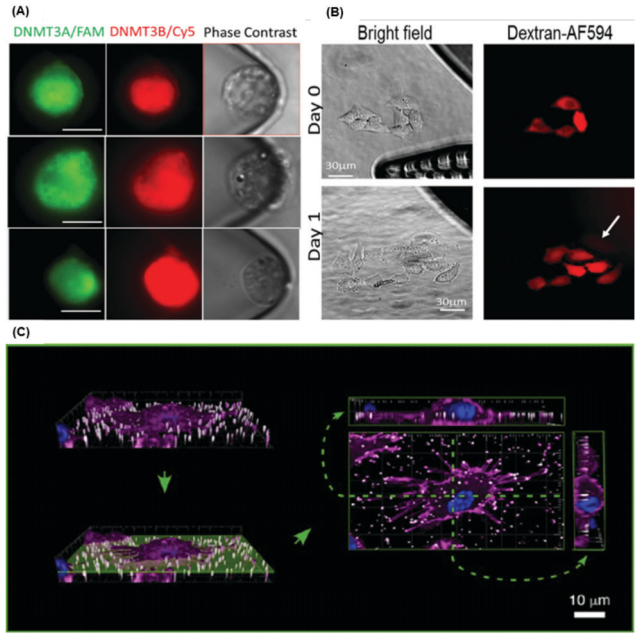

Fig. 16 Nano-electroporation for living cell interrogation by benign detection and perturbation at RNA level. (A) Micrographs of wild-type Kasumi-1 AML cells transfected with DNMT3A/B MBs.[97] Reproduced with permission from Wiley. (B) HeLa cells transfected with MBs and imaged after 24 h of incubation (day 1) showing that the electroporated cells divided.[140] Reproduced with permission from Wiley. (C) Three-dimensional reconstruction (left) of confocal images of mouse bone marrow derived dendritic cells (BMDCs) (membrane: magenta, nucleus: blue) on top of Alexa-labeled NWs (white).[141] Reproduced with permission from ACS.

activity with excellent spatiotemporal resolution. Electroporation-assisted intracellular probing can be achieved not only by deploying various biosensors into the living cells but also by extracting biomolecules of interest from the cells. Lu's group developed a series of microfluidic-based electroporation systems to selectively extract proteins and genes from mammalian cells and bacterial.[89,142]

6. Additional applications of micro-/nanoscale electroporation

In addition to biomedical applications, electroporation has been utilized in a variety of disciplines, including the food industry and microbiology. For instance, pulsed electric field (PEF) electroporation has been reported to significantly improve microorganism inactivation efficiency compared with traditional thermal pasteurization methods.[143,144] PEF has also been used in food processing to induce cell wall breakdown, which facilitates extraction processes from plant cells. For additional discussions on this topic, the reader is referred to more comprehensive reviews on this matter.[144–146]

7. Conclusions and outlook

Micro- and nanoscale technologies have played a fundamental role in the development of advanced non-viral transfection approaches for numerous fundamental and translational applications. Microscale electroporation offers multiple advantages over conventional bulk electroporation approaches, while further miniaturization (*i.e.*, nanoscale-based electroporation) has enabled a host of additional capabilities including dosage control and causing minimum to negligible cell perturbation. Although micro/nano-electroporation platforms hold great promise, it should be noted that most systems require significant expertise and resources from a manufacturing and/or operation standpoint, which could hamper widespread use of these technologies. Further research needs to be conducted in order to develop easily scalable fabrication processes as well as more user friendly operation protocols.

Altogether, micro/nanoscale electroporation approaches are poised to significantly impact both biomedical research and clinical medicine and, as such, warrant further study and proper allocation of resources for successful development. For example, current micro/nanoscale electroporation can successfully deliver cargo into the cytosol, but many gene therapy applications require cargo to be transported into the nucleus for permanent transfection or specific functions. Design of a 'nucleus-target', instead of 'naked' cargo, in combination with efficient electroporation platforms will be highly valuable. There is also great potential to apply *in vivo* MEP/NEP systems for personalized cell therapy, regenerative medicine and gene editing.

Acknowledgements

The authors are grateful to the National Science Foundation (EEC-0914790) for the financial support of this study.

Notes and references

1 P. D. Hsu, E. S. Lander and F. Zhang, *Cell*, 2014, **157**, 1262–1278.
2 J. A. Doudna and E. Charpentier, *Science*, 2014, **346**, DOI: 10.1126/science.1258096.
3 L. Koch, *Nat. Rev. Genet.*, 2016, DOI: 10.1038/nrg.2016.72.
4 N. P. Restifo, M. E. Dudley and S. A. Rosenberg, *Nat. Rev. Immunol.*, 2012, **12**, 269–281.
5 Y. Buganim, D. A. Faddah and R. Jaenisch, *Nat. Rev. Genet.*, 2013, **14**, 427–439.
6 J. B. Gurdon, *Nat. Rev. Mol. Cell Biol.*, 2016, **17**, 137–138.
7 A. El-Sayed and H. Harashima, *Mol. Ther.*, 2013, **21**, 1118–1130.
8 S. Mitragotri, *Adv. Drug Delivery Rev.*, 2013, **65**, 100–103.
9 S. N. Wang and L. J. Lee, *Biomicrofluidics*, 2013, **7**, DOI: 10.1063/1.4774071.
10 T. Geng and C. Lu, *Lab Chip*, 2013, **13**, 3803–3821.
11 P. E. Boukany, A. Morss, W. C. Liao, B. Henslee, H. Jung, X. Zhang, B. Yu, X. Wang, Y. Wu, L. Li, K. Gao, X. Hu, X. Zhao, O. Hemminger, W. Lu, G. P. Lafyatis and L. J. Lee, *Nat. Nanotechnol.*, 2011, **6**, 747–754.
12 L. Nan, Z. D. Jiang and X. Y. Wei, *Lab Chip*, 2014, **14**, 1060–1073.

13 T. Kotnik, W. Frey, M. Sack, S. H. Meglic, M. Peterka and D. Miklavcic, *Trends Biotechnol.*, 2015, **33**, 480–488.
14 Z. G. Yang, L. Q. Chang, C. L. Chiang and L. J. Lee, *Curr. Pharm. Des.*, 2015, **21**, 6081–6088.
15 E. Neumann, M. Schaefer-Ridder, Y. Wang and P. H. Hofschneider, *EMBO J.*, 1982, **1**, 841–845.
16 T. Santra and F. Tseng, *Micromachines*, 2013, **4**, 333.
17 J. Gehl, *Acta Physiol. Scand.*, 2003, **177**, 437–447.
18 T. Kotnik, P. Kramar, G. Pucihar, D. Miklavcic and M. Tarek, *IEEE Elect. Insul. Mag.*, 2012, **28**, 14–23.
19 S. Haberl, D. Miklavcic, G. Sersa, W. Frey and B. Rubinsky, *IEEE Elect. Insul. Mag.*, 2013, **29**, 29–37.
20 M. Rebersek, D. Miklavcic, C. Bertacchini and M. Sack, *IEEE Elect. Insul. Mag.*, 2014, **30**, 8–18.
21 J. C. Weaver, *IEEE Trans. Dielectr. Electr. Insul.*, 2003, **10**, 754–768.
22 T. Y. Tsong, *Biophys. J.*, 1991, **60**, 297–306.
23 S. Y. Ho and G. S. Mittal, *Crit. Rev. Biotechnol.*, 1996, **16**, 349–362.
24 J. C. Weaver and Y. A. Chizmadzhev, *Bioelectrochem. Bioenerg.*, 1996, **41**, 135–160.
25 R. Davalos, Y. Huang and B. Rubinsky, *Microscale Thermophys. Eng.*, 2000, **4**, 147–159.
26 E. Neumann, S. Kakorin and K. Tœnsing, *Bioelectrochem. Bioenerg.*, 1999, **48**, 3–16.
27 R. Stämpfli, *An. Acad. Bras. Cienc.*, 1958, **30**, 57–63.
28 G. Narayanan and M. H. Doshi, *Curr. Urol. Rep.*, 2016, **17**, 15.
29 C. Mansson, R. Brahmstaedt, A. Nilsson, P. Nygren and B. M. Karlson, *Eur. J. Surg. Oncol.*, 2016, **42**, 1401–1406.
30 Y. Zu, S. Huang, W.-C. Liao, Y. Lu and S. Wang, *J. Biomed. Nanotechnol.*, 2014, **10**, 982–992.
31 D. Zhao, D. Huang, Y. Li, M. Wu, W. Zhong, Q. Cheng, X. Wang, Y. Wu, X. Zhou, Z. Wei, Z. Li and Z. Liang, *Sci. Rep.*, 2016, **6**, 18469.
32 F. Kashanchi, J. F. Duvall and J. N. Brady, *Nucleic Acids Res.*, 1992, **20**, 4673–4674.
33 S. O. Choi, Y. C. Kim, J. W. Lee, J. H. Park, M. R. Prausnitz and M. G. Allen, *Small*, 2012, **8**, 1081–1091.
34 W. B. Wang, P. M. Kutny, S. L. Byers, C. J. Longstaff, M. J. DaCosta, C. H. Pang, Y. F. Zhang, R. A. Taft, F. W. Buaas and H. Y. Wang, *J. Genet. Genomics*, 2016, **43**, 319–327.
35 S. Remy, V. Quillaud-Chenouard, L. Tesson, S. Menoret, C. Usal, L. Brusselle, T. H. Nguyen, A. De Cian, C. Giovannangeli, J. P. Concordet and I. Anegon, *Transgenic Res.*, 2016, **25**, 258–258.
36 Y.-C. Lin, C.-M. Jen, M.-Y. Huang, C.-Y. Wu and X.-Z. Lin, *Sens. Actuators, B*, 2001, **79**, 137–143.
37 L. Chang, J. Hu, F. Chen, Z. Chen, J. Shi, Z. Yang, Y. Li and L. J. Lee, *Nanoscale*, 2016, **8**, 3181–3206.
38 S. Wang and L. J. Lee, *Biomicrofluidics*, 2013, **7**, 011301.
39 M. B. Fox, D. C. Esveld, A. Valero, R. Luttge, H. C. Mastwijk, P. V. Bartels, A. Berg and R. M. Boom, *Anal. Bioanal. Chem.*, 2006, **385**, 474–485.
40 W. G. Lee, U. Demirci and A. Khademhosseini, *Integr. Biol.*, 2009, **1**, 242–251.
41 S. Movahed and D. Li, *Microfluid. Nanofluid.*, 2010, **10**, 703–734.
42 M. Wang, O. Orwar, J. Olofsson and S. G. Weber, *Anal. Bioanal. Chem.*, 2010, **397**, 3235–3248.
43 J. Olofsson, K. Nolkrantz, F. Ryttsén, B. A. Lambie, S. G. Weber and O. Orwar, *Curr. Opin. Biotechnol.*, 2003, **14**, 29–34.
44 Y. Huang and B. Rubinsky, *Biomed. Microdevices*, 1999, **2**, 145–150.
45 Y. Huang and B. Rubinsky, *Sens. Actuators, A*, 2001, **89**, 242–249.
46 H. Huang, Z. Wei, Y. Huang, D. Zhao, L. Zheng, T. Cai, M. Wu, W. Wang, X. Ding, Z. Zhou, Q. Du, Z. Li and Z. Liang, *Lab Chip*, 2011, **11**, 163–172.
47 P. Deng, H. Mei and Y. K. Lee, *IEEE NEMS*, 2014, DOI: 10.1109/NEMS.2014.6908815.
48 Y. Li, M. Wu, D. Zhao, Z. Wei, W. Zhong, X. Wang, Z. Liang and Z. Li, *Sci. Rep.*, 2015, **5**, 17817.
49 F. Kupfer, S. M. Lattanzio, M. Maschietto, A. Botos, M. Mahnkopf, J. Bruns, M. Schreiter, S. Vassanelli and R. Thewes, *IEEE IWASI*, 2015, DOI: 10.1109/IWASI.2015.7184936.
50 Y.-C. Lin, M. Li and C.-C. Wu, *Lab Chip*, 2004, **4**, 104–108.
51 Y. Xu, S. Su, C. Zhou, Y. Lu and W. Xing, *Bioelectrochemistry*, 2015, **102**, 35–41.
52 I. Zudans, A. Agarwal, O. Orwar and S. G. Weber, *Biophys. J.*, 2007, **92**, 3696–3705.
53 Y. Huang and B. Rubinsky, *Sens. Actuators, A*, 2003, **104**, 205–212.
54 J. A. Lundqvist, F. Sahlin, M. A. I. Åberg, A. Strömberg, P. S. Eriksson and O. Orwar, *Proc. Natl. Acad. Sci. U. S. A.*, 1998, **95**, 10356–10360.
55 K. Nolkrantz, C. Farre, A. Brederlau, R. I. D. Karlsson, C. Brennan, P. S. Eriksson, S. G. Weber, M. Sandberg and O. Orwar, *Anal. Chem.*, 2001, **73**, 4469–4477.
56 A. Valero, J. N. Post, J. W. van Nieuwkasteele, P. M. ter Braak, W. Kruijer and A. van den Berg, *Lab Chip*, 2008, **8**, 62–67.
57 M. Khine, A. Lau, C. Ionescu-Zanetti, J. Seo and L. P. Lee, *Lab Chip*, 2005, **5**, 38–43.
58 Z. Fei, X. Hu, H.-W. Choi, S. Wang, D. Farson and L. J. Lee, *Anal. Chem.*, 2010, **82**, 353–358.
59 W. Kang, S. S. P. Nathamgari, J. P. Giraldo-Vela, R. L. McNaughton, J. Kessler and H. D. Espinosa, *IEEE Nano*, 2014, DOI: 10.1109/NANO.2014.6968068.
60 C. Ionescu-Zanetti, A. Blatz and M. Khine, *Biomed. Microdevices*, 2007, **10**, 113–116.
61 L. Chang, M. Howdyshell, W.-C. Liao, C.-L. Chiang, D. Gallego-Perez, Z. Yang, W. Lu, J. C. Byrd, N. Muthusamy, L. J. Lee and R. Sooryakumar, *Small*, 2015, **11**, 1818–1828.
62 Y.-C. Chung, Y.-S. Chen and S.-H. Lin, *Sens. Actuators, B*, 2015, **213**, 261–267.
63 Y. Zhan, J. Wang, N. Bao and C. Lu, *Anal. Chem.*, 2009, **81**, 2027–2031.
64 R. Ziv, Y. Steinhardt, G. Pelled, D. Gazit and B. Rubinsky, *Biomed. Microdevices*, 2008, **11**, 95–101.
65 S. C. Bürgel, C. Escobedo, N. Haandbæk and A. Hierlemann, *Sens. Actuators, B*, 2015, **210**, 82–90.

66 G.-B. Lee, C.-J. Chang, C.-H. Wang, M.-Y. Lu and Y.-Y. Luo, *Microsys. Nanoeng.*, 2015, DOI: 10.1038/micronano.2015.7.
67 H.-Y. Wang and C. Lu, *Anal. Chem.*, 2006, **78**, 5158–5164.
68 A. Adamo, A. Arione, A. Sharei and K. F. Jensen, *Anal. Chem.*, 2013, **85**, 1637–1641.
69 J. Wang, M. J. Stine and C. Lu, *Anal. Chem.*, 2007, **79**, 9584–9587.
70 H. Lu, M. A. Schmidt and K. F. Jensen, *Lab Chip*, 2005, **5**, 23–29.
71 Z. Wei, X. Li, D. Zhao, H. Yan, Z. Hu, Z. Liang and Z. Li, *Anal. Chem.*, 2014, **86**, 10215–10222.
72 B. del Rosal, C. Sun, D. N. Loufakis, C. Lu and D. Jaque, *Lab Chip*, 2013, **13**, 3119–3127.
73 T. Geng, Y. Zhan, J. Wang and C. Lu, *Nat. Protoc.*, 2011, **6**, 1192–1208.
74 J. Wang, Y. Zhan, V. M. Ugaz and C. Lu, *Lab Chip*, 2010, **10**, 2057–2061.
75 N. Demierre, T. Braschler, P. Linderholm, U. Seger, H. van Lintel and P. Renaud, *Lab Chip*, 2007, **7**, 355–365.
76 T. Geng, Y. Zhan, H.-Y. Wang, S. R. Witting, K. G. Cornetta and C. Lu, *J. Controlled Release*, 2010, **144**, 91–100.
77 T. Zhu, C. Luo, J. Huang, C. Xiong, Q. Ouyang and J. Fang, *Biomed. Microdevices*, 2009, **12**, 35–40.
78 Z. Wei, D. Zhao, X. Li, M. Wu, W. Wang, H. Huang, X. Wang, Q. Du, Z. Liang and Z. Li, *Anal. Chem.*, 2011, **83**, 5881–5887.
79 D. Selmeczi, T. S. Hansen, Ö. Met, I. M. Svane and N. B. Larsen, *Biomed. Microdevices*, 2011, **13**, 383–392.
80 B. del Rosal, C. Sun, D. N. Loufakis, C. Luc and D. Jaque, *Lab Chip*, 2013, **13**, 3119–3127.
81 Y. H. Zhan, Z. N. Cao, N. Bao, J. B. Li, J. Wang, T. Geng, H. Lin and C. Lu, *J. Controlled Release*, 2012, **160**, 570–576.
82 T. Geng, Y. H. Zhan, H. Y. Wang, S. R. Witting, K. G. Cornetta and C. Lu, *J. Controlled Release*, 2010, **144**, 91–100.
83 H. Y. Wang and C. Lu, *Biotechnol. Bioeng.*, 2006, **95**, 1116–1125.
84 H. Y. Wang and C. Lu, *Anal. Chem.*, 2006, **78**, 5158–5164.
85 T. Geng, Y. H. Zhan, J. Wang and C. Lu, *Nat. Protoc.*, 2011, **6**, 1192–1208.
86 S. Ma, B. Schroeder, C. Sun, D. N. Loufakis, Z. N. Cao, N. Sriranganathan and C. Lu, *Integr Biol-Uk*, 2014, vol. 6, pp. 973–978.
87 C. Sun, Z. N. Cao, M. Wu and C. Lu, *Anal. Chem.*, 2014, **86**, 11403–11409.
88 C. Sun, M. X. Ouyang, Z. N. Cao, S. Ma, H. Alqublan, N. Sriranganathan, Y. X. Wang and C. Lu, *Chem Commun.*, 2014, **50**, 11536–11539.
89 T. Geng, N. Bao, N. Sriranganathanw, L. W. Li and C. Lu, *Anal. Chem.*, 2012, **84**, 9632–9639.
90 Y. H. Zhan, C. Sun, Z. N. Cao, N. Bao, J. H. Xing and C. Lu, *Anal. Chem.*, 2012, **84**, 8102–8105.
91 H. Lambert, R. Pankov, J. Gauthier and R. Hancock, *Biochem. Cell Biol.*, 1990, **68**, 729–734.
92 A. Meir and B. Rubinsky, *RSC Adv.*, 2014, **4**, 54603–54613.
93 S. Movahed and D. Li, *J. Membr. Biol.*, 2012, **246**, 151–160.
94 A. Kaner, I. Braslavsky and B. Rubinsky, *Biomed. Microdevices*, 2013, **16**, 181–189.
95 O. T. Nedelcu, R. Corman, D. Stan and C. M. Mihailescu, *SMICND*, 2015, DOI: 10.1109/SMICND.2015.7355210.
96 P. E. Boukany, A. Morss, W.-C. Liao, B. Henslee, H. Jung, X. Zhang, B. Yu, X. Wang, Y. Wu, L. Li, K. Gao, X. Hu, X. Zhao, O. Hemminger, W. Lu, G. P. Lafyatis and L. J. Lee, *Nat. Nanotechnol.*, 2011, **6**, 747–754.
97 X. Zhao, X. Huang, X. Wang, Y. Wu, A.-K. Eisfeld, S. Schwind, D. Gallego-Perez, P. E. Boukany, G. I. Marcucci and L. J. Lee, *Adv. Sci.*, 2015, **2**, 1500111.
98 K. Gao, L. Li, L. He, K. Hinkle, Y. Wu, J. Ma, L. Chang, X. Zhao, D. G. Perez, S. Eckardt, J. McLaughlin, B. Liu, D. F. Farson and L. J. Lee, *Small*, 2014, **10**, 1015–1023.
99 X. Xie, A. M. Xu, S. Leal-Ortiz, Y. Cao, C. C. Garner and N. A. Melosh, *ACS Nano*, 2013, **7**, 4351–4358.
100 K. Riaz, S. F. Leung, S. Tripathi, G. S. Sethi, H. Shagoshtasbi, Z. Fan and Y. K. Lee, *IEEE NEMS*, 2014, DOI: 10.1109/NEMS.2014.6908779.
101 K. Riaz, S. F. Leung, H. Shagoshtasbi, Z. Fan and Y. K. Lee, *IEEE NEMS*, 2015, DOI: 10.1109/NEMS.2015.7147423.
102 N. Jokilaakso, E. Salm, A. Chen, L. Millet, C. D. Guevara, B. Dorvel, B. Reddy, A. E. Karlstrom, Y. Chen, H. Ji, Y. Chen, R. Sooryakumar and R. Bashir, *Lab Chip*, 2013, **13**, 336–339.
103 T. S. Santra, H.-Y. Chang, P.-C. Wang and F.-G. Tseng, *Analyst*, 2014, **139**, 6249–6258.
104 T. S. Santra, P.-C. Wang, H.-Y. Chang and F.-G. Tseng, *Appl. Phys. Lett.*, 2013, **103**, 233701.
105 W. Kang, F. Yavari, M. Minary-Jolandan, J. P. Giraldo-Vela, A. Safi, R. L. McNaughton, V. Parpoil and H. D. Espinosa, *Nano Lett.*, 2013, **13**, 2448–2457.
106 J. P. Giraldo-Vela, W. Kang, R. L. McNaughton, X. Zhang, B. M. Wile, A. Tsourkas, G. Bao and H. D. Espinosa, *Small*, 2015, **11**, 2386–2391.
107 L. Chang, P. Bertani, D. Gallego-Perez, Z. Yang, F. Chen, C. Chiang, V. Malkoc, T. Kuang, K. Gao, L. J. Lee and W. Lu, *Nanoscale*, 2016, **8**, 243–252.
108 S. Hacein-Bey-Abina, J. Hauer, A. Lim, C. Picard, G. P. Wang, C. C. Berry, C. Martinache, F. Rieux-Laucat, S. Latour, B. H. Belohradsky, L. Leiva, R. Sorensen, M. Debre, J. L. Casanova, S. Blanche, A. Durandy, F. D. Bushman, A. Fischer and M. Cavazzana-Calvo, *N. Engl. J. Med.*, 2010, **363**, 355–364.
109 L. Naldini, *Nature*, 2015, **526**, 351–360.
110 C. E. Thomas, A. Ehrhardt and M. A. Kay, *Nat. Rev. Genet.*, 2003, **4**, 346–358.
111 B. Ferraro, M. P. Morrow, N. A. Hutnick, T. H. Shin, C. E. Lucke and D. B. Weiner, *Clin. Infect. Dis.*, 2011, **53**, 296–302.
112 M. Rosati, A. Valentin, R. Jalah, V. Patel, A. von Gegerfelt, C. Bergamaschi, C. Alicea, D. Weiss, J. Treece, R. Pal, P. D. Markham, E. T. A. Marques, J. T. August, A. Khan, R. Draghia-Akli, B. K. Felber and G. N. Pavlakis, *Vaccine*, 2008, **26**, 5223–5229.
113 L. A. Hirao, L. Wu, A. S. Khan, D. A. Hokey, J. Yan, A. L. Dai, M. R. Betts, R. Draghia-Akli and D. B. Weiner, *Vaccine*, 2008, **26**, 3112–3120.
114 W. Yang, Y. Bai, Y. Xiong, J. Zhang, S. Chen, X. Zheng, X. Meng, L. Li, J. Wang, C. Xu, C. Yan, L. Wang, C. C. Chang,

T. Y. Chang, T. Zhang, P. Zhou, B. L. Song, W. Liu, S. C. Sun, X. Liu, B. L. Li and C. Xu, *Nature*, 2016, **531**, 651–655.

115 M. Caskey, F. Klein, J. C. Lorenzi, M. S. Seaman, A. P. West Jr., N. Buckley, G. Kremer, L. Nogueira, M. Braunschweig, J. F. Scheid, J. A. Horwitz, I. Shimeliovich, S. Ben-Avraham, M. Witmer-Pack, M. Platten, C. Lehmann, L. A. Burke, T. Hawthorne, R. J. Gorelick, B. D. Walker, T. Keler, R. M. Gulick, G. Fatkenheuer, S. J. Schlesinger and M. C. Nussenzweig, *Nature*, 2015, **522**, 487–491.

116 S. A. Rosenberg and N. P. Restifo, *Science*, 2015, **348**, 62–68.

117 Y. B. Zhao, E. Moon, C. Carpenito, C. M. Paulos, X. J. Liu, A. L. Brennan, A. Chew, R. G. Carroll, J. Scholler, B. L. Levine, S. M. Albelda and C. H. June, *Cancer Res.*, 2010, **70**, 9053–9061.

118 C. Rossig and M. K. Brenner, *Mol. Ther.*, 2004, **10**, 5–18.

119 M. Kalos and C. H. June, *Immunity*, 2013, **39**, 49–60.

120 A. Varela-Rohena, C. Carpenito, E. E. Perez, M. Richardson, R. V. Parry, M. Milone, J. Scholler, X. Hao, A. Mexas, R. G. Carroll, C. H. June and J. L. Riley, *Immunol. Res.*, 2008, **42**, 166–181.

121 L. Chang, D. Gallego-Perez, X. Zhao, P. Bertani, Z. Yang, C. L. Chiang, V. Malkoc, J. Shi, C. K. Sen, L. Odonnell, J. Yu, W. Lu and L. J. Lee, *Lab Chip*, 2015, **15**, 3147–3153.

122 A. Khvorova, A. Reynolds and S. D. Jayasena, *Cell*, 2003, **115**, 209–216.

123 L. Chang, D. Gallego-perez, C. Chiang, P. Bertani, T. Kuang, F. Chen, Y. Sheng, Z. Chen, J. Shi, H. Yang, V. Malkoc, W. Lu and L. J. Lee, *Small*, 2016, DOI: 10.1002/smll.201601465.

124 A. Fire, S. Xu, M. K. Montgomery, S. A. Kostas, S. E. Driver and C. C. Mello, *Nature*, 1998, **391**, 806–811.

125 J. Tabernero, G. I. Shapiro, P. M. LoRusso, A. Cervantes, G. K. Schwartz, G. J. Weiss, L. Paz-Ares, D. C. Cho, J. R. Infante, M. Alsina, M. M. Gounder, R. Falzone, J. Harrop, A. C. White, I. Toudjarska, D. Bumcrot, R. E. Meyers, G. Hinkle, N. Svrzikapa, R. M. Hutabarat, V. A. Clausen, J. Cehelsky, S. V. Nochur, C. Gamba-Vitalo, A. K. Vaishnaw, D. W. Sah, J. A. Gollob and H. A. Burris, 3rd, *Cancer Discovery*, 2013, **3**, 406–417.

126 D. Gallego-Perez, J. J. Otero, C. Czeisler, J. Ma, C. Ortiz, P. Gygli, F. P. Catacutan, H. N. Gokozan, A. Cowgill, T. Sherwood, S. Ghatak, V. Malkoc, X. Zhao, W. C. Liao, S. Gnyawali, X. Wang, A. F. Adler, K. Leong, B. Wulff, T. A. Wilgus, C. Askwith, S. Khanna, C. Rink, C. K. Sen and L. J. Lee, *Nanomedicine*, 2016, **12**, 399–409.

127 K. Gao, X. Huang, C. L. Chiang, X. Wang, L. Chang, P. Boukany, G. Marcucci, R. Lee and L. J. Lee, *Mol. Ther.*, 2016, **24**, 956–964.

128 R. Maresch, S. Mueller, C. Veltkamp, R. Ollinger, M. Friedrich, I. Heid, K. Steiger, J. Weber, T. Engleitner, M. Barenboim, S. Klein, S. Louzada, R. Banerjee, A. Strong, T. Stauber, N. Gross, U. Geumann, S. Lange, M. Ringelhan, I. Varela, K. Unger, F. Yang, R. M. Schmid, G. S. Vassiliou, R. Braren, G. Schneider, M. Heikenwalder, A. Bradley, D. Saur and R. Rad, *Nat. Commun.*, 2016, **7**, 10770.

129 V. T. Chu, T. Weber, B. Wefers, W. Wurst, S. Sander, K. Rajewsky and R. Kuhn, *Nat. Biotechnol.*, 2015, **33**, 543–548.

130 K. Takahashi and S. Yamanaka, *Cell*, 2006, **126**, 663–676.

131 Saijilafu, E. M. Hur and F. Q. Zhou, *Nat. Commun.*, 2011, DOI: 10.1038/ncomms1568.

132 M. dal Maschio, D. Ghezzi, G. Bony, A. Alabastri, G. Deidda, M. Brondi, S. S. Sato, R. P. Zaccaria, E. Di Fabrizio, G. M. Ratto and L. Cancedda, *Nat. Commun.*, 2012, **3**, 960.

133 J. L. Pinyon, S. F. Tadros, K. E. Froud, Y. W. AC, I. T. Tompson, E. N. Crawford, M. Ko, R. Morris, M. Klugmann and G. D. Housley, *Sci. Transl. Med.*, 2014, **6**, 233–254.

134 R. Phillips, *Physical biology of the cell*, Garland Science, New York, NY, Second edn., 2013.

135 L. Chang, J. Hu, F. Chen, Z. Chen, J. Shi, Z. Yang, Y. Li and L. J. Lee, *Nanoscale*, 2016, **8**, 3181–3206.

136 C. Xie, Z. Lin, L. Hanson, Y. Cui and B. Cui, *Nat. Nanotechnol.*, 2012, **7**, 185–190.

137 L. Hanson, W. Zhao, H. Y. Lou, Z. C. Lin, S. W. Lee, P. Chowdary, Y. Cui and B. Cui, *Nat. Nanotechnol.*, 2015, **10**, 554–562.

138 F. Santoro, S. Dasgupta, J. Schnitker, T. Auth, E. Neumann, G. Panaitov, G. Gompper and A. Offenhausser, *ACS Nano*, 2014, **8**, 6713–6723.

139 K. Kitamura, B. Judkewitz, M. Kano, W. Denk and M. Hausser, *Nat. Methods*, 2008, **5**, 61–67.

140 J. P. Giraldo-Vela, W. Kang, R. L. McNaughton, X. Zhang, B. M. Wile, A. Tsourkas, G. Bao and H. D. Espinosa, *Small*, 2015, **11**, 2386–2391.

141 A. K. Shalek, J. T. Gaublomme, L. Wang, N. Yosef, N. Chevrier, M. S. Andersen, J. T. Robinson, N. Pochet, D. Neuberg, R. S. Gertner, I. Amit, J. R. Brown, N. Hacohen, A. Regev, C. J. Wu and H. Park, *Nano Lett.*, 2012, **12**, 6498–6504.

142 Y. H. Zhan, V. A. Martin, R. L. Geahlen and C. Lu, *Lab Chip*, 2010, **10**, 2046–2048.

143 S. Mahnic-Kalamiza, E. Vorobiev and D. Miklavcic, *J. Membr. Biol.*, 2014, **247**, 1279–1304.

144 G. Saulis, *Food Eng. Rev.*, 2010, **2**, 52–73.

145 T. Tryfona and M. T. Bustard, *Biotechnol. Bioeng.*, 2006, **93**, 413–423.

146 B. M. Chassy, A. Mercenier and J. Flickinger, *Trends Biotechnol.*, 1988, **6**, 303–309.

